THE JOURNAL OF PHYSICAL CHEMISTRY B

Feature Article

pubs.acs.org/JPCB

Interpretation of IR and Raman Line Shapes for H_2O and D_2O Ice Ih

L. Shi, S. M. Gruenbaum, and J. L. Skinner*

Theoretical Chemistry Institute and Department of Chemistry, University of Wisconsin, Madison, Wisconsin 53706, United States

ABSTRACT: Noticeable differences between the vibrational (IR and Raman) spectra of neat H_2O and D_2O ice Ih are observed experimentally. Here, we employ our theoretical mixed quantum/classical approach to investigate these differences. We find reasonable agreement between calculated and experimental line shapes at both high and low temperatures. From understanding the structure of ice Ih and its vibrational exciton Hamiltonian, we provide assignments of the IR and Raman spectral features for both H_2O and D_2O ice Ih. We find that in H_2O ice these features are due to strong and weak intermolecular coupling, not to intramolecular coupling. The differences between H_2O and D_2O ice spectra are attributed to the significantly stronger intramolecular coupling in D_2O ice. Our conclusion for both H_2O and D_2O ice is that the molecular symmetric and antisymmetric normal modes do not form a useful basis for understanding OH or OD stretch spectroscopy.

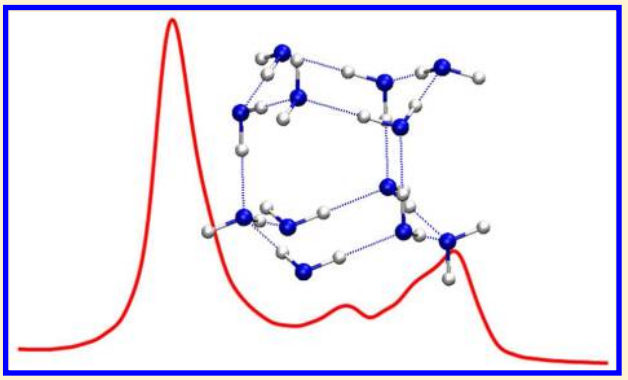

I. INTRODUCTION

Ice, with its 15 thermodynamically stable phases, has been an exciting research topic for decades.[1,2] Its complicated phase diagram reflects a diversity of molecular interactions and hydrogen-bond topologies. In ice Ih, the stable phase under ambient conditions, the oxygen atoms form a hexagonal lattice and the hydrogen atom positions are disordered, which is termed proton disorder in the literature.[2] This proton disorder in ice Ih is responsible for many of its interesting elastic, thermal, and electrical properties.[2] Proton disorder also affects the lattice dynamical properties of the crystal, as measured by IR, Raman, and inelastic neutron scattering.[2] Since the water OH stretch frequency is very sensitive to its local environment, vibrational spectroscopy in this region has been widely used to provide insight into the structure and dynamics of ice Ih.[3−20] Many experiments have been conducted on dilute HOD in either H_2O or D_2O, in which cases the effects of vibrational coupling to the OD or OH stretch, respectively, are negligible.[3,4,6,9,11,12,15,17,19] The advantage of these systems is that the experimental line shapes directly reflect the distributions of the OH (OD) local environments; however, the vibrational spectroscopy of neat H_2O or D_2O ice is significantly richer and may provide some additional information on the structure and dynamics in ice Ih. In this paper, we will focus on neat H_2O and D_2O.

In neat ice Ih, there are several competing factors determining the line shapes from the viewpoint of condensed phase molecular spectroscopy. Proton disorder causes additional heterogeneity of OH (OD) local site vibrational frequencies compared with a proton-ordered phase. Thermal motion also adds additional heterogeneity, which, however, can be narrowed spectroscopically.[21] In the isolated (gas-phase) molecule, intramolecular vibrational coupling produces symmetric and antisymmetric stretch normal mode eigenstates. In the crystal, there are also intermolecular vibrational couplings that tend to delocalize further the eigenstates. Finally, there are additional couplings to lower frequency (bend and lattice vibration) modes. The IR and Raman spectra themselves are quite complex, with multiple peaks and shoulders.[10] The most sophisticated experiments involve polarized and depolarized Raman scattering from single-crystal ice.[9,22]

When one makes the isotopic substitution from H to D in water, the stretch and bend vibrational frequencies decrease dramatically. Surprisingly, however, the intensities and patterns of the spectral peaks are also quite different in H_2O and D_2O ice.[10] There are three possible reasons that this might be. First, there are nuclear quantum effects in liquid and solid water arising from the substantial dispersion in the ground-state vibrational wave function, and these quantum effects are more pronounced in H_2O than in D_2O (because of the lighter hydrogen mass). Second, the Fermi resonance between the bend overtone and symmetric stretch is stronger for D_2O than in H_2O. Third, the intramolecular coupling is stronger in D_2O than in H_2O. In this paper, we focus on the intramolecular coupling as a possible source of the spectral differences.

A number of theoretical efforts have been made to interpret ice spectra in the past 40 years,[10,16,23−31] including recent works in our group.[32−34] Whalley[10] summarized progress in the assignments of spectral features prior to 1977. The lowest-frequency peak in the ice Raman spectra was assigned to the globally in-phase symmetric stretch, and the rest of the features resulted from the out-of-phase symmetric and antisymmetric

Received: June 16, 2012
Revised: September 27, 2012
Published: October 12, 2012

ACS Publications © 2012 American Chemical Society

dx.doi.org/10.1021/jp3059239 | J. Phys. Chem. B 2012, 116, 13821−13830

stretches with longitudinal and transverse optical (LO−TO) phonon splitting.[10] Rice and collaborators published a series of theoretical papers on this topic shortly thereafter.[23−27] They employed a model Hamiltonian including many factors mentioned above (e.g., modulation of the OH (OD) stretch frequency, intra- and intermolecular couplings, Fermi resonance, etc.). They attributed most features in the spectra of neat ice to the interplay between intra- and intermolecular couplings and argued that the Fermi resonance was a second-order effect that has more influence on the spectra of D_2O ice Ih.[26,27] In fact, they concluded that the assignment of the spectral features to the molecular symmetric and antisymmetric stretch modes "may be meaningless".[23] They also thought that the LO−TO splitting had little effect on the OH (OD) stretch vibrational line shapes of ice Ih.[26,27] About two decades later, Buch and Devlin proposed a tetrahedral basic unit to interpret the spectra of ice Ih.[16] A similar theoretical study was later carried out by Wójcik and collaborators.[28] Researchers are also beginning to employ ab initio molecular dynamics methods to calculate vibrational spectra of ice Ih.[29,31] These approaches are promising, but they typically underestimate the OH (OD) stretching frequency.

Recently, our group interpreted ice spectra using the mixed quantum/classical vibrational exciton approach[35] and found that the intermolecular couplings between the nearest-neighbor local-mode OH chromophores determine most spectral features of H_2O ice Ih.[33,34] In particular, in our model, unlike in the gas phase, the intramolecular coupling in H_2O ice is almost zero, certainly much smaller than the width of the local frequency distribution (diagonal disorder) and typical intermolecular couplings. Thus, we concur with Rice and co-workers that interpretation of the spectra in terms of the molecular symmetric and antisymmetric stretches is not appropriate for H_2O ice Ih.[33] We assigned the peaks in the spectra as arising from "strong" and "weak" intermolecular coupling. As mentioned above, experimental spectra for D_2O ice are somewhat different from that for H_2O.[10] We had not analyzed this situation in any detail.[33,34]

The very recent and detailed experimental paper by Shigenari and Abe[22] on IR and polarization-resolved Raman spectra for single crystal ice Ih, and its corresponding low-temperature proton-ordered phase ice XI, provides new and important data. From our point of view, perhaps the most interesting finding is that the unpolarized Raman spectra for these two phases are quite similar, even though one is proton-disordered and the other is not. From this, it would appear that the effect of proton disorder is minimal in the stretch spectroscopy of ice Ih and, therefore, that the spectra can be interpreted using the full symmetry of the hexagonal lattice. In particular, Shigenari and Abe interpret their spectra in terms of the in-phase and out-of-phase symmetric and antisymmetric stretch vibrations.[22] Note, however, that the IR spectra for the ordered (XI) and disordered (Ih) phases are quite different (especially in terms of the peak intensities and widths; see Figure 16 in ref 22), further confusing the situation.

At this point, then, there are two main puzzles: how to understand the differences in the IR and Raman spectra between H_2O and D_2O ice Ih and how to understand the similarities in the Raman spectra, but differences in the IR spectra, between H_2O ice Ih and ice XI. In this paper, we will attempt to address the former in detail, and only comment briefly on the latter. In doing so, we make slight revisions in our theoretical approach,[32−34] we extend our calculations to include Raman scattering from polycrystalline samples, and we consider the temperature dependence of line shapes. The paper is organized as follows. In Section II, we outline our methodology for the spectral calculations; in Section III, we compare our calculated spectra to experiment; in Section IV, we analyze our theoretical spectra and provide assignments of the experimental spectral peaks for both H_2O and D_2O; and in Section V, we conclude.

II. THEORETICAL METHODS

The first step in the calculation of theoretical spectra for ice is the selection of a water model. Here we employ the explicit three-body (E3B) rigid water model recently developed in our group.[36,37] The functional form of the potential is given in ref 36 and was validated by ab initio (MP2) calculations on water dimers and trimers. Note that the E3B model employed here has parameters somewhat different from the one used in previous work.[32,33,36] The E3B model successfully reproduces many properties of liquid water, among them a better freezing point compared with the SPC/E and TIP4P models.[37] The E3B model also reproduces the experimentally observed low-frequency positive peak in the sum-frequency-generation spectrum of the water liquid/vapor interface, in contrast to two-body potentials such as the TIP4P model.[38−40]

For the initial configuration of proton-disordered ice Ih, we employ the 432-molecule configuration generated by Hayward and Reimer.[41] A molecular dynamics simulation of ice Ih is then performed in the NVT ensemble at 245 K using GROMACS version 3.3,[42] modified for the E3B potential. The simulation box is scaled to give the experimental lattice constants at 245 K.[2] Simulations are performed using the SETTLE constraint algorithm[43] with a 1 fs time step, and a Berendsen thermostat is employed with a 0.5 ps coupling constant for production runs.[44] Periodic boundary conditions are applied, the cutoff for Lennard-Jones interaction is set to 0.95 nm, and particle-mesh Ewald[45,46] is used to compute the electrostatic interactions. The atomic coordinates are saved every 2 fs in the production run for the spectral calculations. Molecular dynamics simulations are also performed at 100 and 10 K for spectral calculations using corresponding experimental lattice constants.[2]

To calculate both IR and Raman line shapes, we will use the mixed quantum/classical approach previously developed in our group,[35] in which the high-frequency OH (OD) stretches are treated quantum mechanically, the bends are frozen, and all other molecular degrees of freedom are treated classically via conventional molecular dynamics. As detailed in our previous work, the environmental dependence of the water stretching frequencies, transition dipoles, and transition polarizabilities are parametrized from B3LYP/6-311++G** calculations on water clusters as a function of the component of the electric field, E, at the location of the water hydrogen atom along the OH (OD) bond direction.[32−34] Because E3B water has the same geometry and point charges as TIP4P,[47] we will utilize previously developed TIP4P-based maps in the spectral calculations. These maps for the water stretching frequencies (anharmonic 0−1 transition frequencies) and other quantities are given in Table 1 of ref 32.

The dipole derivative (μ') map determined in ref 32 shows significant curvature as a function of E, whereas previous maps developed for SPC/E water were linear in the electric field.[48] In addition, the number of configurations used for the fit was rather small. We repeated these calculations, using many more

(roughly 2000) water clusters, and reparameterized the quadratic fit. For each (randomly chosen) cluster of water molecules from a liquid simulation, the central OH bond was stretched, keeping the center of mass of the molecule fixed, and the total system dipole was calculated as discussed previously[32] as a function of the stretching coordinate. The dipole derivative μ' is then given as the magnitude of the derivative of the vector dipole, and the results for each water cluster are plotted versus the electric field, E, as the blue points in Figure 1. The black

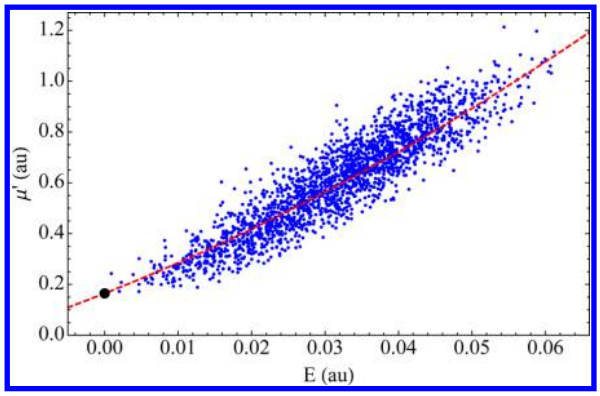

Figure 1. Quantum calculations of the dipole derivative μ' (in au) plotted as a function of electric field for bulk water clusters (blue circles) and gas-phase water (black circle). The red dashed line is a quadratic fit to the data, eq 1.

point indicates the gas-phase value of μ'. We fit the data to a quadratic function of E, where $\mu'(E = 0)$ is constrained to equal the calculated gas-phase value of 0.1646 au. The resulting fit for μ' is shown as the red curve in Figure 1 and is given by

$$\mu' = 0.1646 + 11.39E + 63.41E^2 \tag{1}$$

where both E and μ' are given in atomic units. The fit in eq 1 has a root-mean-squared deviation (RMSD) of 0.078 au, compared with an RMSD value of 0.092 au for the previous μ' map described in ref 32.

In the local-mode basis, the intramolecular coupling ω_{ij}^a between the two OH (OD) stretches on the same molecule is approximated as[49]

$$\hbar\omega_{ij}^a = k_{ij}^a x_i x_j + \frac{\cos(\phi)}{m_O} p_i p_j \tag{2}$$

where k_{ij}^a is the mixed second derivative of the potential energy with respect to both bond lengths, evaluated at the minimum; x_i is the 0−1 position matrix element (using the anharmonic states) of the stretch coordinate for local mode i; p_i is the corresponding 0−1 momentum matrix element; ϕ is the HOH (DOD) bond angle (ϕ = 104.52 for E3B water[37]); and m_O is the oxygen mass. k_{ij}^a, x_i, and p_i all depend on the molecule's environment. In our parametrization,[33,34] k_{ij}^a is linear in the electric fields E_i and E_j. Substituting the TIP4P map for k_{ij}^a and the values of ϕ and m_O into eq 2, the intramolecular coupling is given by[34]

$$\omega_{ij}^a = (-1361 + 27165(E_i + E_j))x_i x_j - 1.887 p_i p_j \tag{3}$$

Note that the coupling is in wavenumbers, and all other quantities are in atomic units. The position and momentum matrix elements have been parametrized in terms of the local-mode frequencies.[33] For example, for a gas-phase molecule, setting $E_i = E_j = 0$ and using the gas-phase local-mode frequency of 3707 cm^{-1} to determine the gas-phase matrix elements, we find[34] the intramolecular coupling to be −49.8 and −54.3 cm^{-1}, respectively, for H_2O and D_2O, in reasonable agreement with experiment (−49.4 and −59.3 cm^{-1}).

We assume transition dipole intermolecular coupling between chromophores i and j, given by

$$\hbar\omega_{ij}^e = \frac{\mu'_i\mu'_j\{\hat{u}_i\cdot\hat{u}_j - 3[(\hat{u}_i\cdot\hat{n}_{ij})(\hat{u}_j\cdot\hat{n}_{ij})]\}}{r_{ij}^3} x_i x_j \tag{4}$$

where $\hat{u}$ is the unit vector in the OH (OD) direction, $\hat{n}_{ij}$ is the unit vector along the line connecting the two point dipoles, and r_{ij} is the distance between these point dipoles. (This form comes from the standard dipole−dipole interaction energy, expanding each dipole to first order in position, and then taking the appropriate matrix elements.) The only free parameter is then the location of the point dipole, and this location was previously parametrized to be 0.67 Å from the oxygen atom along the OH (OD) bond.[33] Because we are now using a different map for the transition dipole, eq 1, this changes our values of the intermolecular coupling, which could either improve or worsen the agreement of the transition dipole model with the ab initio calculations. To investigate this, in Figure 2, we compare our calculated intermolecular couplings

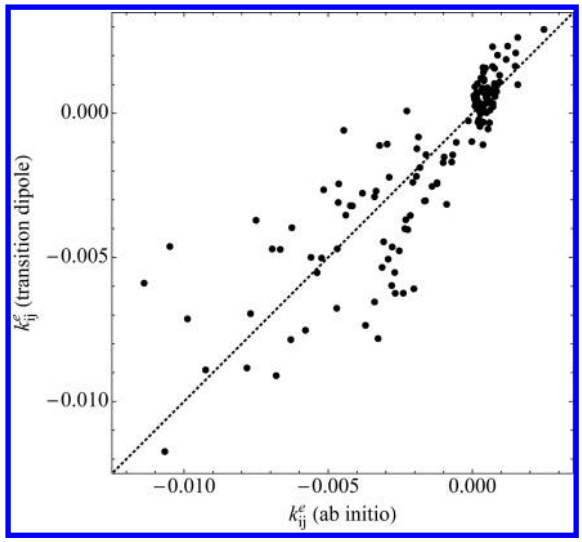

Figure 2. Comparison of ab initio calculated intermolecular couplings k_{ij}^e versus transition dipole couplings from eq 4. The dotted line indicates the diagonal.

using the transition dipole approximation with the ab initio results from ref 33. In fact, the agreement is improved over that in ref 33: the new RMSD is 0.0016 au compared with the previous RMSD of 0.0019 au.

For an aligned single crystal, the polarizations of the light electric field can be chosen to be along the a, a', or c crystal axes, leading to three IR spectra, three polarized Raman spectra, and three depolarized Raman spectra. The formulas we use to calculate these spectra are given in ref 33. The lifetime is taken to be 300 (700) fs for H_2O (D_2O) ice.[33,50] For polycrystalline samples, one needs to average over the orientations of the crystal axes with respect to the lab-fixed axes. This has been worked out by McQuarrie,[51] and the formulas we use to calculate spectra in these cases are given in the Appendix.

dx.doi.org/10.1021/jp3059239 | J. Phys. Chem. B 2012, 116, 13821−13830

III. RESULTS AND COMPARISON WITH EXPERIMENT

In Figure 3, we plot experimental polarized (*cc* and *aa*) and depolarized (*aa′* and *ca*) Raman spectra for single crystal H_2O and D_2O ice Ih at 269 K.[9] The polarized spectra have a low-frequency main peak and two features at higher frequency, whereas the depolarized spectra show only the higher frequency peaks. The peak frequencies are indicated by the vertical dashed lines. The differences between the D_2O and H_2O spectra are 3-fold: (1) the overall D_2O spectra are significantly narrower, (2) the peaks are sharper for D_2O, and (3) the spacing between the peaks is even for H_2O, but not so for D_2O. In the same figure, we also show our theoretical spectra. Despite the slight refinements (new μ' map, reparameterized E3B model) we have made in our model and spectral calculations, in fact, these results are very similar to our previous results.[33,34] The features of the experimental spectra are reproduced qualitatively by our calculations. The theoretical frequencies are also given by vertical dashed lines (they are all slightly too blue compared with experiment).

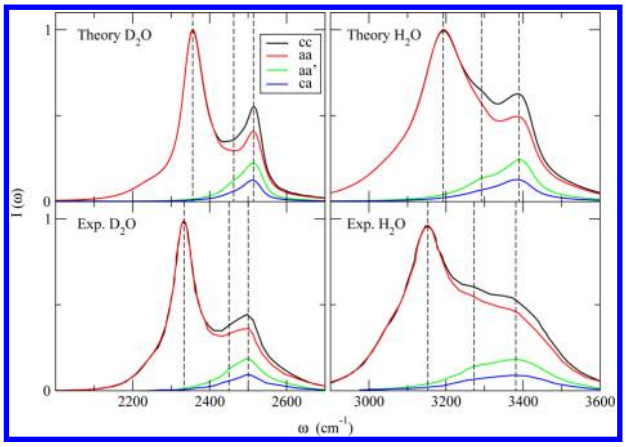

Figure 3. Theoretical (E3B model at 245 K, top) and experimental[9] (at 269 K, bottom) polarized (*cc* and *aa*) and depolarized (*aa′* and *ca*) Raman line shapes for single crystal D_2O (left) and H_2O (right) ice Ih. The vertical dashed lines indicate the frequencies of the different transitions.

Next, we consider the IR and unpolarized Raman spectra of neat H_2O and D_2O polycrystalline ice Ih at 100 K. In Figure 4, we show experimental spectra (black lines).[10] The Raman spectra again have three peaks, but now, the middle peak is more pronounced. The spacings between the peaks are more or less as above, but all peaks are slightly red-shifted at this lower temperature. The IR spectra also have three peaks; the lowest frequency peak is more pronounced in D_2O. In each case, the higher two frequency peaks correspond to the higher two Raman peaks, and the lower frequency peak is blue-shifted from the lower frequency Raman peak. Thus, there appear to be four distinct transitions, which are present to greater or lesser extent in IR or Raman spectra. This experimental situation is indicated by the four vertical dashed lines for each isotope. In the same figure, we also show our theoretical calculations; theory is again in qualitative agreement with experiment, although the theoretical H_2O IR spectrum does not exhibit the highest frequency peak.

We have also performed theoretical calculations at 10 K, at which temperature the spectra sharpen up and are easier to interpret. (Note that the equilibrium phase at 10 K is ice XI,[2] but one can still study supercooled ice Ih at this temperature,

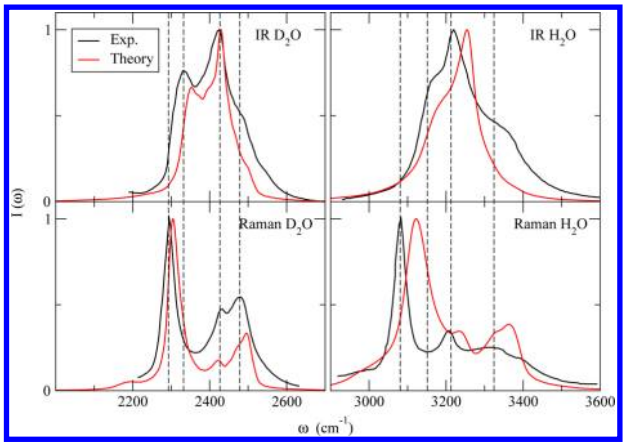

Figure 4. Theoretical (E3B model) and experimental IR (top) and unpolarized Raman (bottom) line shapes for polycrystalline D_2O (left) and H_2O (right) ice Ih at 100 K. Experimental line shapes are taken from ref 10. The dashed vertical lines indicate the frequencies of the four experimental transitions.

both experimentally and theoretically.) We show the evolution of the theoretical polarized (*cc*) Raman, depolarized (*aa′*) Raman, and polycrystalline IR line shapes, as a function of temperature, for H_2O and D_2O ice Ih in Figures 5 and 6. The frequencies of the four peaks, in all spectra taken together, are shown as the vertical dashed lines for each temperature. All lines blue shift with increasing temperature, and the spacings remain roughly the same. To summarize then, for both H_2O and D_2O, there appear to be four transitions, labeled from red to blue, 1 to 4. Peaks 1, 3, and 4 are Raman-active, and peaks 2, 3, and 4 are IR-active.

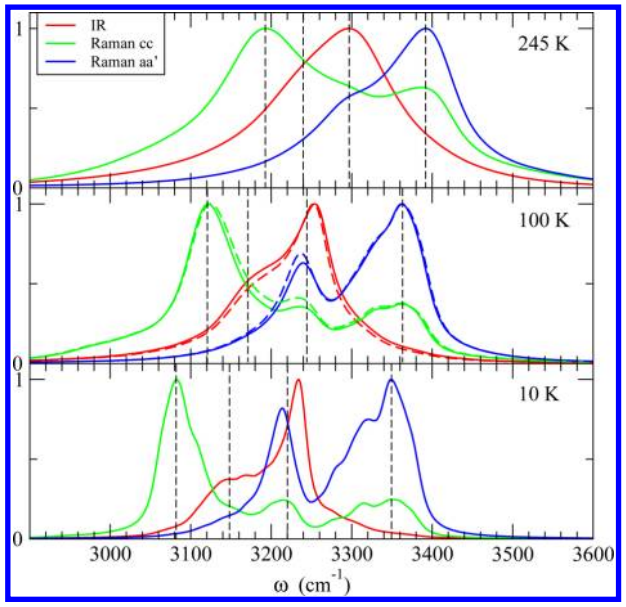

Figure 5. Theoretical line shapes for H_2O ice Ih at 245, 100, and 10 K (from top to bottom). The red lines are the (polycrystalline) IR line shapes, the green lines are the Raman *cc* line shapes, and the blue lines are the Raman *aa′* line shapes. The three line shapes are normalized to the same peak height. The dashed lines in the 100 K panel are calculated line shapes setting the intramolecular coupling to 0. The vertical dashed lines are the frequencies of the four transitions at each temperature.

dx.doi.org/10.1021/jp3059239 | J. Phys. Chem. B 2012, 116, 13821−13830

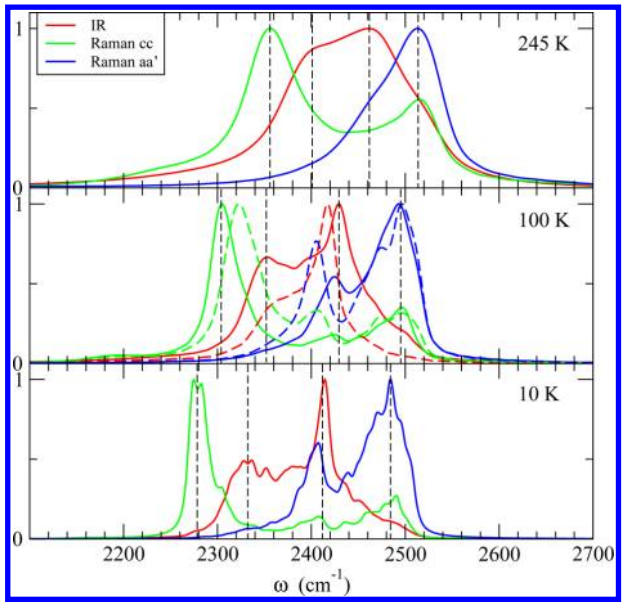

Figure 6. Same as Figure 5, but for D_2O ice Ih.

In Figures 7 and 8, we plot all available experimental data for the frequencies of these four peaks as a function of temperature.

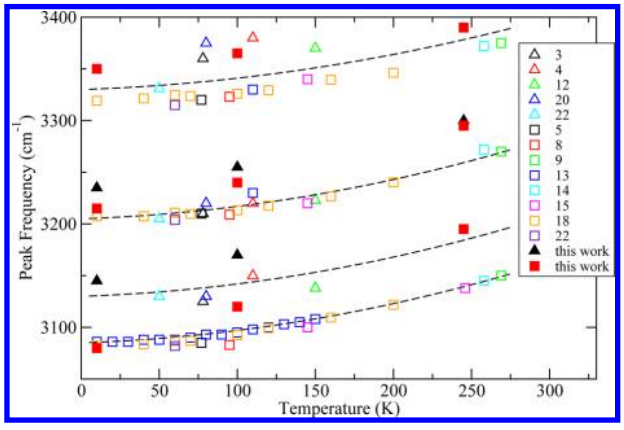

Figure 7. Temperature dependence of peak frequencies for H_2O ice Ih. The triangles are from IR line shapes, and the squares are from Raman line shapes. Open symbols are from experimental line shapes with reference number in the legend, and solid symbols are from calculated line shapes. The dashed lines are guides to the eye for the experimental data.

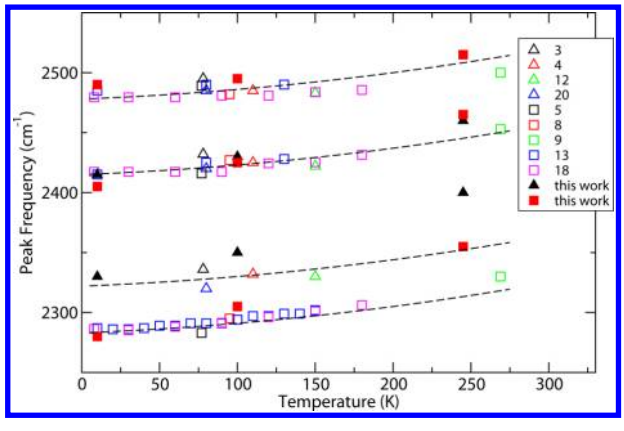

Figure 8. Same as Figure 7, but for D_2O ice.

The open squares are Raman (polarized, depolarized, or unpolarized; single crystal or polycrystalline) experimental results, and the open triangles are IR (polycrystalline) experimental results. For each transition, the dashed lines are guides to the eye, to see the temperature dependence. From these graphs, one can see how the spacing of the lines differs for H_2O and D_2O. For each isotope, we also plot our theoretical results (from Figures 5 and 6) as the solid squares for Raman transitions 1, 3, and 4, and solid triangles for IR transitions 2 and 3. The theoretical results show the same trends as experiment but are uniformly somewhat too blue.

IV. SPECTRAL INTERPRETATION AND DISCUSSION

With the success of our model in qualitatively reproducing several experimental spectra, we can attempt to understand the differences between the line shapes of H_2O and D_2O ice Ih and to interpret their spectral features. The properties and nature of the vibrational eigenstates and their selection rules reflect the competing effects in the exciton Hamiltonian of diagonal (frequency) disorder due to the proton-disordered environments of the local chromophores, intramolecular coupling, the various kinds of intermolecular coupling, and thermal disorder. We can minimize the effect of the latter by focusing here on results at 10 K.

As a first step, let us quantify the extent of diagonal disorder. The diagonal elements of our exciton Hamiltonian are the local OH (OD) stretch 0−1 transition frequencies, which are sensitive to hydrogen bonding and local environments. In ice Ih, all water molecules are tetrahedrally hydrogen-bonded (with two donors and two acceptors) to four nearest neighbors, which produces no dispersion in the frequency distribution. If we consider the configuration of the hydrogen-bonding partner of a specific OH, however, one finds that there are four distinct classes"[53] on the basis of the relative orientations of hydrogen-bonded donor and acceptor, as shown in Figure 9. The

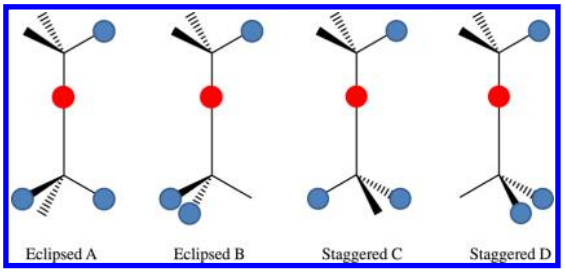

Figure 9. Four possible hydrogen-bonding dimers in ice Ih based on the relative orientations of the hydrogen bond donor and acceptor. The red and blue circles are hydrogen atoms in the dimer. The hydrogen bonds in the eclipsed dimers (A and B) are along the *c* axis of ice Ih; the hydrogen bonds in the staggered dimers (C and D) are along a direction oblique to the *c* axis.

hydrogen bonds in the eclipsed dimers (A and B) are along the *c* axis of ice Ih, whereas those in the staggered dimers (C and D) are along a direction oblique to the *c* axis.[53] These motifs can be visualized from the 12-molecule fragment of ice Ih shown in Figure 10, where the *c* axis is vertical and the dotted lines are hydrogen bonds.

We can decompose the site frequency distribution into contributions from each class, as shown in Figure 11 for ice Ih at 10 K. The relative area of the distribution for each class reflects the statistical percentage of that class in Ice Ih, which in our configuration is very close to the percentage assuming the

dx.doi.org/10.1021/jp3059239 | J. Phys. Chem. B 2012, 116, 13821−13830

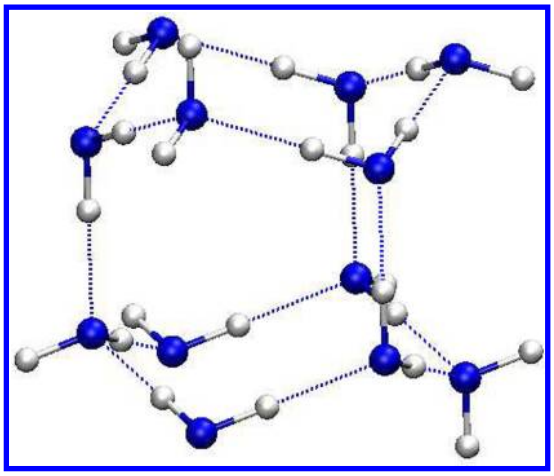

Figure 10. Twelve-molecule fragment of ice Ih. The *c* axis is vertical, and the dotted lines are hydrogen bonds.

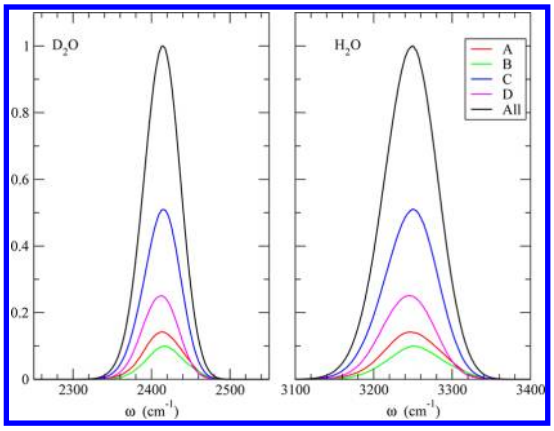

Figure 11. Calculated local OH (OD) stretch frequency distributions for the four classes of OH (OD) bonds in ice Ih and their sum at 10 K. Left panel is for D_2O; right panel is for H_2O.

proton disorder is locally random (A: 1/6; B: 1/12; C: 1/2; D: 1/4). The frequency distributions of each class are very similar, indicating that this is not an important source of diagonal disorder. This is not consistent with the claim of two different kinds of hydrogen bonds in ice,[52,54] but is consistent with the refutation[55,56] of this claim. The widths of the frequency distributions for each class are mainly due to the proton-disordered environments of each dimer, but the imperfect tetrahedral hydrogen bond network of E3B water molecules (with HOH angles of 104.52°, not 109.47°) and residual thermal motions at 10 K also contribute. A noticeable difference between H_2O and D_2O ice Ih is that the site frequency distribution of D_2O (~55 cm^{-1}) is narrower than that of H_2O (~80 cm^{-1}) at 10 K, which partially explains the difference in the line widths of H_2O and D_2O vibrational spectra. These differences have to do with the difference in scale between OH and OD stretch frequencies, whose ratio is approximately related to the square root of the ratio of the relevant reduced masses (which is roughly $\sqrt{2}$).

We next consider the off-diagonal elements of the Hamiltonian, the vibrational couplings. Intramolecular couplings are calculated using eq 3, and intermolecular couplings are calculated within the interacting transition dipole approximation, eq 4. To understand the intermolecular couplings, we plot in Figure 12 the radial distribution function

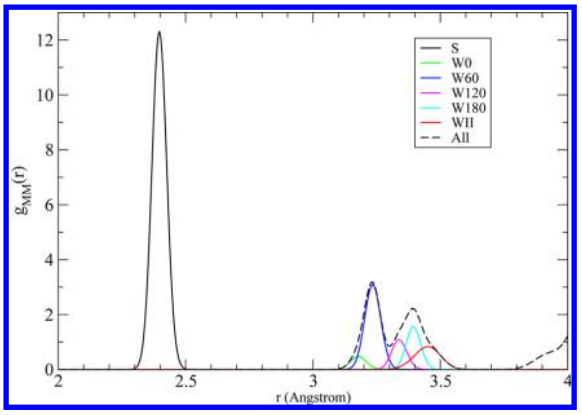

Figure 12. Calculated radial distribution function of the dipole positions for OH stretches in ice Ih and its decomposition into the six classes of pairs in H_2O ice Ih at 10 K. The dipole position of the OH chromophore is located at 0.67 Å from the oxygen atom along the OH bond.[33].

of the point dipole positions, $g_{MM}(r)$ (M designates point dipole position), for ice Ih at 10 K. The dipolar couplings within 3.6 Å in $g_{MM}(r)$ are grouped into six classes, shown in Figure 13. Again, to understand these classes, it may be helpful

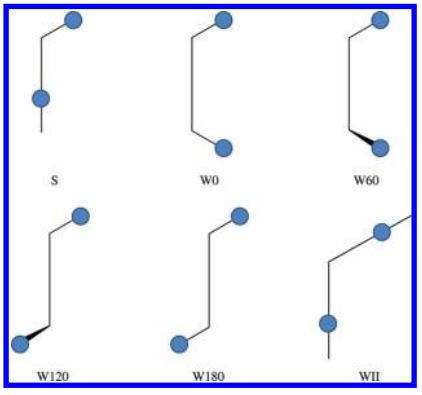

Figure 13. Six possible classes of dipolar couplings between two OH chromophores within 3.6 Å at 10 K. Blue circles are the two hydrogen atoms in the pair. The oxygen atoms are represented by the vertices.

to consult Figure 10. The nearest OH pairs are ~2.4 Å apart, denoted as S (for strong). Four types of pairs are similar in terms of distances (from 3.1 to 3.5 Å) and are all within the first solvation shell of the hydrogen bond donor water molecule. They are denoted as W0, W60, W120, and W180 (W for weak), in which the numerals are the dihedral angles formed by the two OH bonds. The final class, denoted as WII, is for molecules in the second solvation shell of the hydrogen bond donor water molecule (II means the second solvation shell); however, point dipoles in the WII pairs are not far away from each other (~3.45 Å apart) in the imperfect tetrahedral hydrogen bond network of E3B water molecules.

In Figure 14, we plot the distributions of intermolecular couplings as well as intramolecular couplings for both H_2O and D_2O at 10 K. The S pairs lead to the strongest (in magnitude) intermolecular couplings (about −40 cm^{-1} for H_2O). The dipolar intermolecular coupling is affected not only by the distance between two transition dipoles, but also by their relative orientations (see eq 3), and so nearer pairs do not necessarily have stronger coupling. In fact, relatively distant WII coupling pairs show the largest positive couplings in the

dx.doi.org/10.1021/jp3059239 | J. Phys. Chem. B 2012, 116, 13821−13830

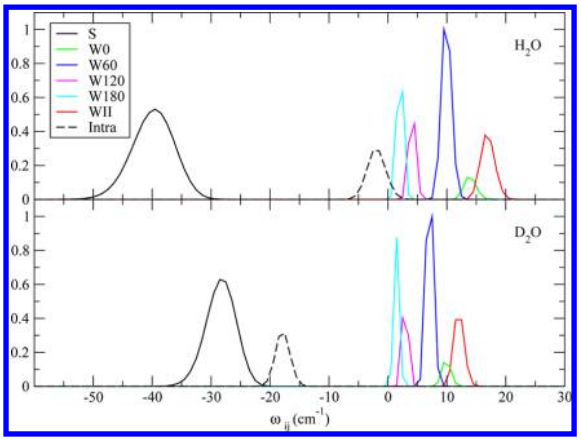

Figure 14. Calculated distributions of dipolar intermolecular couplings within 3.6 Å and intramolecular coupling for H_2O (top) and D_2O (bottom) ice Ih at 10 K.

Hamiltonian. As we have seen before,[33,34] the intramolecular couplings in H_2O are relatively small, peaked at -3 cm^{-1}. Given that the diagonal disorder in the Hamiltonian for H_2O at 10 K is ∼80 cm^{-1}, one may anticipate that the intramolecular couplings will not significantly change the vibrational density of states, whereas the intermolecular couplings may introduce splittings. The widths of the coupling distributions arise primarily from the intrinsic structural heterogeneity due to the proton disorder and imperfect tetrahedral hydrogen bond network of E3B, rather than residual thermal motions at 10 K.

The coupling distributions for D_2O (bottom panel of Figure 14) are quite different from those for H_2O. The intermolecular couplings (S pairs: on the order of -28 cm^{-1}; WII pairs: 12 cm^{-1}) are smaller in magnitude for D_2O, whereas the intramolecular couplings (-18 cm^{-1}) are much larger. These can be qualitatively understood from eqs 2 and 4: for a harmonic oscillator, the position matrix element x is proportional to the square root of the reduced mass of the oscillator, and the momentum matrix element p is inversely proportional to the square root.[57] The intermolecular couplings in eq 4 depend on x, but not p, so a smaller reduced mass leads to a larger coupling magnitude for H_2O. In eq 2, for intramolecular couplings, k^a_{ij} is usually positive, and $\cos(\phi)/m_O$ is negative. It is the competition between the two terms in eq 2 that results in more negative intramolecular couplings for D_2O. Because the diagonal disorder in the Hamiltonian for D_2O at 10 K is about ∼55 cm^{-1}, we can expect that in D_2O, both inter- and intramolecular couplings will introduce splittings in the OD stretch vibrational density of states (see below).

With a better understanding of the exciton Hamiltonian for H_2O and D_2O, we next investigate the effects of these couplings on the OH (OD) vibrational frequency distribution.[33] The top (bottom) panel in Figure 15 shows the vibrational frequency distribution with various couplings for H_2O (D_2O) at 10 K. We begin by showing the frequency distribution when all vibrational coupling is neglected; these are the black curves, which are identical to those in Figure 11. Next, we include only the intramolecular coupling for each molecule and then diagonalize the Hamiltonian for each configuration, which produces the red lines. For H_2O, this coupling does essentially nothing, since the magnitude of the coupling is small compared with the width of the diagonal disorder, whereas for D_2O, where the intramolecular coupling is much larger, it splits the peak significantly. Next, we remove the intramolecular coupling

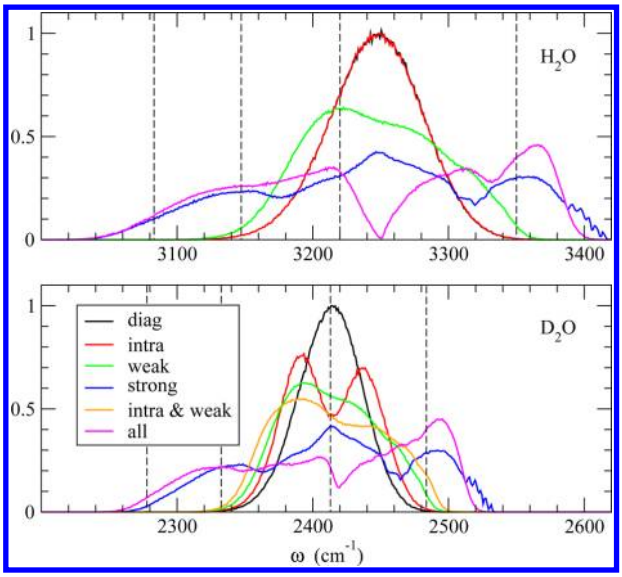

Figure 15. Theoretical frequency distributions of H_2O and D_2O ice Ih at 10 K. The black lines are the local OH (OD) stretch frequency distributions. The red lines include only the intramolecular couplings. The green lines include only the "weak" intermolecular couplings. The blue lines include only the "strong" intermolecular couplings. The orange line includes only the intramolecular and weak intermolecular couplings. The magenta lines include all couplings. The dashed vertical lines are the frequencies at 10 K from Figures 5 and 6 and are labeled from left to right as C, SL, W (W/I), and SH in H_2O (D_2O) ice.

and include intermolecular coupling involving all pairs with separations greater than 3 Å (that is, we include all the "weak" couplings). These results are shown by the green curves. The effect of these weak couplings is similar for both H_2O and D_2O, broadening the frequency distribution, with the highest amplitude on the low-frequency side. For D_2O, we next include both intramolecular and weak coupling to obtain the orange curve, which shows that the intramolecular coupling further broadens the frequency distibution, but the highest amplitude is still on the low-frequency side. We next remove the weak and intramolecular coupling and now include only the strong couplings, which results in the blue curves. These show dramatic perturbations from the diagonal distributions because these strong couplings are on the order of the width of the diagonal disorder. One sees that the strong couplings substantially broaden the distributions (but less so for D_2O, since the couplings are smaller). Finally, if one includes all couplings, one obtains the magenta lines. For both H_2O and D_2O, each of these curves has three main peaks: about 3140, 3220, and 3360 cm^{-1} for H_2O and 2320, 2410, and 2490 cm^{-1} for D_2O. Comparing the magenta, blue, and green curves for H_2O, one can reasonably conclude that these three peaks arise from strong, weak, and strong interactions, respectively, which we denote SL (L is for low-frequency), W, and SH (H is for high), respectively. For D_2O, one compares the magenta, blue, and orange curves, similarly labeling the three peaks as SL, W/I (I is for intramolecular), SH.

The frequency distributions are related to spectra but are, of course, not the same thing, since the latter are weighted by the square of the transition dipoles or polarizability and also have dynamical and lifetime effects. Still, one would expect to see signatures of the frequency distribution in the spectra, to different extents for the different kinds of line shapes. In Figures 5 and 6, we showed vertical dashed lines for the four peaks in

dx.doi.org/10.1021/jp3059239 | J. Phys. Chem. B 2012, 116, 13821−13830

the different spectra for each of the temperatures and isotopes. In Figure 15, we also show these same four dashed lines for 10 K for each isotope. In each case, the three higher-frequency lines correspond roughly to the peaks in the frequency distribution, which we label as SL, W (W/I), and SH for H_2O (D_2O). For each isotope, the lowest frequency line occurs where the frequency distribution is actually quite small. The transition appears only in polarized Raman spectra, where, as discussed earlier,[10,16,23,24,28,33,58] the intensity is enhanced by the constructive interference of many in-phase transitions, which we denote as C for collective. In summary, then, the four transitions 1, 2, 3, and 4, are designated C, SL, W (W/I), and SH for H_2O (D_2O). Transition 1 occurs in the polarized Raman (it is the main peak), transition 2 is in the IR, and transitions 3 (which is the main peak in the IR) and 4 appear in all spectra.

Certainly for H_2O, our results show that the intramolecular coupling makes essentially no contribution to the spectroscopy. To make this very clear, in Figure 5, we show theoretical Raman and IR line shapes for 100 K where the intramolecular coupling has been set to 0; one sees essentially no change. Since the intermolecular couplings are so much larger than the intramolecular couplings, this implies that the basis of the symmetric and antisymmetric molecular eigenstates is not useful or relevant for understanding the spectra. This is in agreement with our previous analysis[33] and with earlier work by Rice and co-workers[23] but in disagreement with the recent intrepretation by Shigenari and Abe.[22] For D_2O, the intramolecular coupling is clearly much more important (see the results for no intramolecular coupling at 100 K in Figure 6), and it changes the spacing among the four transitions and their intensities. Still, the qualitative features of the spectra do not change from H_2O to D_2O, and so our conclusion is that here, too, the molecular eigenstates are not relevant.

With regard to the temperature dependence of the theoretical line shapes in Figures 5 and 6, higher temperatures lead to larger amplitudes of the low-frequency motions, which on average weakens hydrogen bonds, producing a blue shift in the frequencies. In addition, the larger range of configurations sampled at higher temperatures broadens the lines. Obtaining the correct frequency for the C (collective) line is particularly difficult for us, since it is collective (and not related to specific more local vibrational eigenstates), and indeed, one sees in Figures 7 and 8 that we do not predict the temperature dependence of the peak frequency for this (lowest-frequency) transition very well.

Finally, we can discuss the role of proton disorder in the spectroscopy of ice Ih and ice XI. Our results indicate that proton disorder in ice Ih produces substantial diagonal disorder in the exciton Hamiltonian, which affects the eigenstates, transition strengths, and the spectroscopy. Still, our previous inverse participation ratio analysis shows that the vibrational eigenstates are extended,[33] meaning that the amount of diagonal disorder is not large enough to localize the states. Therefore, it may be reasonable that spectra for proton-ordered ice XI are qualitatively similar to those for ice Ih. In addition, note that OH stretches in ice XI are not all equivalent, and therefore, their frequencies will not be the same. So even though the system is ordered, the different diagonal frequencies may to some extent mimic the diagonal disorder in ice Ih (in that in both cases, the diagonal frequencies are distributed). In addition, we must keep in mind that the IR spectra for these two crystals are not particularly similar.[22]

V. CONCLUSIONS

The work presented and discussed here complements our previous work on the IR and Raman spectra of neat H_2O ice Ih.[33,34] With our new E3B water model,[37] we further validate our mixed quantum/classical approach for calculating high-frequency OH (OD) spectra of neat ice Ih by comparing our calculations to experimental spectra at different temperatures, including Raman spectra of polycrystalline ice Ih. Reasonable agreement is found between calculated and experimental line shapes. Through investigation into the structure and frequency distributions for both H_2O and D_2O, we find that it is the stronger intramolecular couplings that change the spectral features (spacings and widths) in D_2O, and it is primarily the smaller "strong" intermolecular couplings that make the line shapes for D_2O narrower compared with H_2O, in agreement with Rice and co-workers' results.[26] On the basis of these, we have suggested assignments for the experimental peaks for both H_2O and D_2O. Our assignments are based on understanding the strong and weak intermolecular couplings and intramolecular couplings on the basis of local OH (OD) stretches, rather than on the basis of molecular symmetric and antisymmetric stretches.[10,22] Large intermolecular couplings and diagonal disorder make molecular symmetric and antisymmetric stretches not useful as a basis for spectral interpretations.

The model is not without its shortcomings. These include: (1) Ice Ih should have nuclear quantum effects.[59−61] Classical molecular dynamics does not describe the spatial delocalization of hydrogen (deuterium) positions in Ice Ih,[62] which will potentially affect the line width, and the classical treatment of lattice librations at low temperature is not well justified. (2) The Fermi resonance between OH (OD) stretches and bending overtones is neglected in our model. This effect has been studied extensively by both experiments[63,64] and theory.[25−27] It is thought that the effects of Fermi resonance in D_2O ice is likely to be more profound than for H_2O,[26] so the peaks at ∼2425 and ∼2485 cm^{-1} in the experimental Raman spectra at 100 K may have contributions from Fermi resonance. (3) In terms of the spectroscopic modeling, the use of the transition bond polarizability model might contribute to the overestimation of the intensity of high-frequency modes in Raman spectra. Transition dipole coupling is not necessarily a good approximation for the nearest OH pairs. Actually, many researchers[16,26,28] treat these couplings differently from longer range intermolecular couplings. Finally, our frequency maps may not be particularly accurate, since they were parametrized from liquid water.[32,33] Nonetheless, our model appears to be good enough to help us understand most of the qualitative spectral features in both H_2O and D_2O ice Ih.

Recent years have seen exciting nonlinear ultrafast experiments performed on ice. Transient hole-burning in HOD/D_2O was first performed by Graener and co-workers.[65] Transient absorption in HOD/D_2O and anisotropic pump−probe decay for H_2O/D_2O mixtures in ice Ih have been measured recently by Bakker and collaborators.[50,66] 2D IR spectroscopy of both isotope-diluted and neat ice Ih have been measured by Hamm and collaborators.[19,20] Sum-frequency-generation spectroscopy on the ice/air interface has been measured by Shultz and collaborators.[67,68] We hope to apply our methodology to understand these nonlinear vibrational experiments in the future. In addition, the new experiments on ice XI[22] and experiments on amorphous ices[27,69,70] provide further oppor-

tunities for us to test and refine our models and to obtain information about structure and dynamics in these fascinating solid water phases.

VII. APPENDIX

For a polycrystalline sample, the crystallites have all possible orientations with respect to the lab-fixed coordinate system. Equivalently, when using a simulation of a single crystal to calculate spectroscopy for polycrystalline samples, one must average over all possible orientations of the lab-fixed axes with respect to the crystal axes. For IR spectroscopy, the simple result is that one must sum over the three Cartesian polarizations of the single crystal. Thus, within the mixed quantum/classical approach,[71,72] the IR line shape function can be written as[33]

$$I(\omega) \sim \mathrm{Re} \int_0^\infty \mathrm{e}^{-i\omega t} \sum_p \sum_{ij} \langle m_{ip}(0)\, F_{ij}(t)\, m_{jp}(t)\rangle \mathrm{e}^{-t/2T_1} \tag{5}$$

where m_{ip} is the pth Cartesian component of the 0−1 transition dipole of the ith chromophore in the simulation-box frame, and T_1 is the lifetime of an OH (OD) stretch. F_{ij} is the matrix element of the time-evolution operator in the site basis, which satisfies the equation

$$\dot{F}(t) = iF(t)\,\kappa(t) \tag{6}$$

subject to the initial condition that $F_{ij}(0) = \delta_{ij}$. $\kappa(t)$ is a matrix with transition frequencies along the diagonal and couplings as off-diagonal elements.[33,72]

Similarly, the line shape functions for the polarized (VV) and depolarized (VH) Raman spectrum within the mixed quantum/classical approach[71,72] can be written as[51]

$$I_{\mathrm{VV}}(\omega) \sim Re \int_0^\infty \mathrm{e}^{-i\omega t} \frac{1}{15} \sum_{pq} \sum_{ij} \langle a_{ipp}(0)\, F_{ij}(t)\, a_{jqq}(t) + 2a_{ipq}(0)\, F_{ij}(t)\, a_{jpq}(t)\rangle \mathrm{e}^{-t/2T_1} \tag{7}$$

and

$$I_{\mathrm{VH}}(\omega) \sim Re \int_0^\infty \mathrm{e}^{-i\omega t} \frac{1}{30} \sum_{pq} \sum_{ij} \langle 3a_{ipq}(0)\, F_{ij}(t)\, a_{jpq}(t) - a_{ipp}(0) F_{ij}(t)\, a_{jqq}(t)\rangle \mathrm{e}^{-t/2T_1} \tag{8}$$

where a_{ipq} is the pq element of the 0−1 transition polarizability tensor of the ith chromophore in the simulation-box frame. Note that the summation over p and q includes $p = q$. Finally, the line shape function for unpolarized Raman is simply

$$I(\omega) = I_{\mathrm{VV}}(\omega) + I_{\mathrm{VH}}(\omega) \tag{9}$$

AUTHOR INFORMATION

Corresponding Author

*E-mail: skinner@chem.wisc.edu.

Notes

The authors declare no competing financial interest.

Biographies

Liang Shi received his B.S. degree in Chemistry from the University of Science and Technology of China in 2009. He is currently working as a graduate student with Professor James L. Skinner at the University of Wisconsin−Madison. His research focuses on understanding the structure and dynamics of ice using theoretical spectroscopy approaches.

Scott M. Gruenbaum graduated from Miami University in 2005 with a B.S. in Chemistry and Mathematics. He received his Ph.D. in Chemistry in 2010 from Cornell University, working with Professor Roger F. Loring on the semiclassical calculation of nonlinear vibrational response functions. In 2010, he joined the group of Professor James L. Skinner at the University of Wisconsi−Madison as a postdoctoral researcher, where he currently studies the vibrational spectroscopy of hydration water in complex environments, such as in lipid bilayers. His other research interests include quantum dynamics and vibrational energy flow in molecules.

James L. Skinner received his Ph.D. from Harvard with Prof. Peter Wolynes in 1979 and then did postdoctoral work with Hans Andersen at Stanford. He is currently the Joseph O. and Elizabeth S. Hirschfelder Professor of Chemistry and Director of the Theoretical Chemistry Institute at the University of Wisconsin. His research interests involve the structure, dynamics, relaxation, and spectroscopy of condensed-phase systems.

■ ACKNOWLEDGMENTS

This work was supported by NSF Grant CHE-1058752. Computations were supported in part by NSF Grant CHE-0840494. The authors are grateful to Dr. Fu Li for helpful discussions.

■ REFERENCES

(1) Salzmann, C. G.; Radaelli, P. G.; Mayer, E.; Finney, J. L. *Phys. Rev. Lett.* **2009**, *103*, 105701.
(2) Petrenko, V. F.; Whitworth, R. W. *Physics of Ice*; Oxford University Press: Oxford, 1999.
(3) Haas, C.; Hornig, D. F. *J. Chem. Phys.* **1960**, *32*, 1763−1769.
(4) Bertie, J. E.; Whalley, E. *J. Chem. Phys.* **1964**, *40*, 1637−1645.
(5) Taylor, M. J.; Whalley, E. *J. Chem. Phys.* **1964**, *40*, 1660−1664.
(6) Ford, T.; Falk, M. *Can. J. Chem.* **1968**, *46*, 3579−3586.
(7) Bertie, J. E.; Labbé, H. J.; Whalley, E. *J. Chem. Phys.* **1969**, *50*, 4501−4520.
(8) Wong, P.; Whalley, E. *J. Chem. Phys.* **1975**, *62*, 2418−2425.
(9) Scherer, J. G.; Snyder, R. G. *J. Chem. Phys.* **1977**, *67*, 4794−4811.
(10) Whalley, E. *Can. J. Chem.* **1977**, *55*, 3429−3441.
(11) Sivakumar, T. C.; Schuh, D.; Sceats, M. G.; Rice, S. A. *Chem. Phys. Lett.* **1977**, *48*, 212−218.
(12) Bergren, M. S.; Schuh, D.; Sceats, M. G.; Rice, S. A. *J. Chem. Phys.* **1978**, *69*, 3477−3482.
(13) Sivakumar, T. C.; Rice, S. A.; Sceats, M. G. *J. Chem. Phys.* **1978**, *69*, 3468−3476.
(14) Sivakumar, T. C.; Chew, H. A. M.; Johari, G. P. *Nature* **1978**, *275*, 524−525.
(15) Minceva-Sukarova, B.; Sherman, W. F.; Wilkinson, G. R. *J. Phys. C: Solid State Phys.* **1984**, *17*, 5833−5850.
(16) Buch, V.; Devlin, J. P. *J. Chem. Phys.* **1999**, *110*, 3437−3443.
(17) Iglev, H.; Schmeisser, M.; Simeonidas, K.; Thaller, A.; Laubereau, A. *Nature* **2006**, *439*, 183−186.
(18) Furic′, K.; Volovšek, V. *J. Mol. Struct.* **2010**, *976*, 174−180.
(19) Perakis, F.; Widmer, S.; Hamm, P. *J. Chem. Phys.* **2011**, *134*, 204505.
(20) Perakis, F.; Hamm, P. *Phys. Chem. Chem. Phys.* **2012**, *14*, 6250−6256.
(21) Kubo, R. *Adv. Chem. Phys.* **1969**, *15*, 101−127.
(22) Shigenari, T.; Abe, K. *J. Chem. Phys.* **2012**, *136*, 174504.
(23) McGraw, R.; Madden, W. G.; Rice, S. A.; Sceats, M. G. *Chem. Phys. Lett.* **1977**, *48*, 219−226.
(24) McGraw, R.; Madden, W.; Bergren, M.; Rice, S. *J. Chem. Phys.* **1978**, *69*, 3483−3496.
(25) Sceats, M. G.; Stavola, M.; Rice, S. A. *J. Chem. Phys.* **1979**, *71*, 983−990.
(26) Bergren, M. S.; Rice, S. A. *J. Chem. Phys.* **1982**, *77*, 583−602.
(27) Rice, S.; Bergren, M.; Belch, A.; Nielson, N. *J. Phys. Chem.* **1983**, *87*, 4295−4308.
(28) Wójcik, M. J.; Szczeponek, K.; Ikeda, S. *J. Chem. Phys.* **2002**, *117*, 9850−9857.
(29) Iftimie, R.; Tuckerman, M. E. *J. Chem. Phys.* **2005**, *122*, 214508.
(30) Buch, V.; Milet, A.; Vácha, R.; Jungwirth, P.; Devlin, J. P. *Proc. Natl. Acad. Sci. U.S.A.* **2007**, *104*, 7342−7347.
(31) Chen, W.; Sharma, M.; Resta, R.; Galli, G.; Car, R. *Phys. Rev. B* **2008**, *77*, 245114.
(32) Li, F.; Skinner, J. L. *J. Chem. Phys.* **2010**, *132*, 204505.
(33) Li, F.; Skinner, J. L. *J. Chem. Phys.* **2010**, *133*, 244504.
(34) Li, F.; Skinner, J. L. *J. Chem. Phys.* **2011**, *134*, 099901.
(35) Skinner, J. L.; Auer, B. M.; Lin, Y.-S. *Adv. Chem. Phys.* **2009**, *142*, 59−103.
(36) Kumar, R.; Skinner, J. L. *J. Phys. Chem. B* **2008**, *112*, 8311−8318.
(37) Tainter, C. J.; Pieniazek, P. A.; Lin, Y.-S.; Skinner, J. L. *J. Chem. Phys.* **2011**, *134*, 184501.
(38) Pieniazek, P. A.; Tainter, C. J.; Skinner, J. L. *J. Am. Chem. Soc.* **2011**, *133*, 10360−10363.
(39) Pieniazek, P. A.; Tainter, C. J.; Skinner, J. L. *J. Chem. Phys.* **2011**, *135*, 044701.
(40) Stiopkin, I. V.; Weeraman, C.; Pieniazek, P. A.; Shalhout, F. Y.; Skinner, J. L.; Benderskii, A. V. *Nature* **2011**, *474*, 192−195.
(41) Hayward, J.; Reimers, J. *J. Chem. Phys.* **1997**, *106*, 1518−1529.
(42) van der Spoel, D.; Lindahl, E.; Hess, B.; van Buuren, A. R.; Apol, E.; Meulenhoff, P. J.; Tieleman, D. P.; Sijbers, A. L. T. M.; Feenstra, K. A.; van Drunen, R.; Berendsen, H. J. C. *Gromacs User Manual version 3.3*; 2005, www.gromacs.org.
(43) Miyamoto, S.; Kollman, P. A. *J. Comput. Chem.* **1992**, *13*, 952−962.
(44) Berendsen, H. J. C.; Postma, J. P. M.; van Gunsteren, W. F.; DiNola, A.; Haak, J. R. *J. Chem. Phys.* **1984**, *81*, 3684−3690.
(45) Darden, T.; York, D.; Pedersen, L. *J. Chem. Phys.* **1993**, *98*, 10089−10092.
(46) Essmann, U.; Perera, L.; Berkowitz, M. L.; Darden, T.; Lee, H.; Pedersen, L. G. *J. Chem. Phys.* **1995**, *103*, 8577−8593.
(47) Jorgensen, W. L.; Chandrasekhar, J.; Madura, J. D.; Impey, R. W.; Klein, M. L. *J. Chem. Phys.* **1983**, *79*, 926−935.
(48) Auer, B. M.; Kumar, R.; Schmidt, J. R.; Skinner, J. L. *Proc. Natl. Acad. Sci. U.S.A.* **2007**, *104*, 14215−14220.
(49) Wilson, E. B.; Decius, J. C.; Cross, P. C. *Molecular Vibrations*; Dover: New York, 1980.
(50) Timmer, R. L. A.; Bakker, H. J. *J. Phys. Chem. A* **2010**, *114*, 4148−4155.
(51) McQuarrie, D. A. *Statistical Mechanics*; Harper and Row: New York, 1976.
(52) Li, J.-C.; Ross, D. K. *Nature* **1993**, *365*, 327−329.
(53) Rick, S. W. *J. Chem. Phys.* **2005**, *122*, 094504.
(54) Li, J. C.; Bennington, S. M.; Ross, D. K. *Phys. Lett. A* **1994**, *192*, 295−300.
(55) Tse, J. S.; Klug, D. D. *Phys. Lett. A* **1995**, *198*, 464−466.
(56) Klotz, S.; Strassle, T.; Salzmann, C. G.; Philippe, J.; Parker, S. F. *Europhys. Lett.* **2005**, *72*, 576−582.
(57) Sakurai, J. J. *Modern Quantum Mechanics*, revised ed.; Addison-Wesley: New York, 1994.
(58) Yang, M.; Skinner, J. L. *Phys. Chem. Chem. Phys.* **2010**, *12*, 982−991.
(59) Ramírez, R.; Herrero, C. P. *Phys. Rev. B* **2011**, *84*, 064130.
(60) Waheed, Q.; Edholm, O. *J. Chem. Theory Comput.* **2011**, *7*, 2903−2909.
(61) Pamuk, B.; Soler, J. M.; Ramírez, R.; Herrero, C. P.; Stephens, P. W.; Allen, P. B.; Fernández-Serra, M.-V. *Phys. Rev. Lett.* **2012**, *108*, 193003.
(62) Herrero, C. P.; Ramírez, R. *J. Chem. Phys.* **2011**, *134*, 094510.
(63) Ritzhaupt, G.; Devlin, J. P. *J. Chem. Phys.* **1977**, *67*, 4779−4780.
(64) Hernandez, J.; Uras, N.; Devlin, J. P. *J. Chem. Phys.* **1998**, *108*, 4525−4529.
(65) Seifert, G.; Weidlich, K.; Graener, H. *Phys. Rev. B* **1997**, *56*, R14231−R14234.
(66) Dokter, A.; Bakker, H. *J. Chem. Phys.* **2008**, *128*, 024502.
(67) Groenzin, H.; Li, I.; Shultz, M. J. *J. Chem. Phys.* **2008**, *128*, 214510.
(68) Barnett, I. L.; Groenzin, H.; Shultz, M. J. *J. Phys. Chem. A* **2011**, *115*, 6039−6045.
(69) Klug, D. D.; Mishima, O.; Whalley, E. *J. Chem. Phys.* **1987**, *86*, 5323−5328.
(70) Kanno, H.; Tomikawa, K.; Mishima, O. *Chem. Phys. Lett.* **1998**, *293*, 412−416.
(71) Auer, B. M.; Skinner, J. L. *J. Chem. Phys.* **2007**, *127*, 104105.
(72) Auer, B. M.; Skinner, J. L. *J. Chem. Phys.* **2008**, *128*, 224511.